Applied Surface Science 257 (2011) 8887–8893

Contents lists available at ScienceDirect

Applied Surface Science

journal homepage: www.elsevier.com/locate/apsusc

Nanomechanical characteristics of annealed Si/SiGe superlattices

Ming-Jhang Wu[a], Hua-Chiang Wen[b,*], Shyh-Chi Wu[a,c], Ping-Feng Yang[d], Yi-Shao Lai[d], Wen-Kuang Hsu[b], Wen-Fa Wu[e], Chang-Pin Chou[a]

[a] Department of Mechanical Engineering, National Chiao Tung University, Hsinchu 300, Taiwan, ROC
[b] Department of Materials Science and Engineering, National Tsing Hua University, Hsinchu 300, Taiwan, ROC
[c] Chung Shan Institute of Science and Technology, CSIST, Taoyuan 325, Taiwan, ROC
[d] Central Labs, Advanced Semiconductor Engineering, Inc., 26 Chin 3rd Rd., Nantze Export Processing Zone, 811 Nantze, Kaohsiung, Taiwan, ROC
[e] National Nano Device Laboratories, Hsinchu 300, Taiwan, ROC

ARTICLE INFO

Article history:
Received 22 February 2011
Received in revised form 3 May 2011
Accepted 3 May 2011
Available online 11 May 2011

Keywords:
Superlattices
Ultrahigh-vacuum chemical vapor deposition
Atomic force microscopy
Transmission electron microscopy

ABSTRACT

In this study, the nanomechanical damage was investigated on the annealed Si/SiGe strained-layer superlattices (SLSs) deposited using an ultrahigh-vacuum chemical vapor deposition (UHVCVD). Nanoscratch, nanoindenter, atomic force microscopy (AFM), and transmission electron microscopy (TEM) techniques were used to determine the nanomechanical behavior of the SiGe films. With a constant force applied, greater hardness number and larger coefficients of friction (μ) were observed on the samples that had been annealed at 600 °C, suggesting that annealing of the Si/SiGe SLSs can induce greater shear resistance. AFM morphological studies of the Si/SiGe SLSs revealed that pile-up phenomena occurred on both sides of each scratch, with the formation of some pellets and microparticles. The Si/SiGe SLSs that had been subjected to annealing under various conditions exhibited significantly different features in their indentation results. Indeed, the TEM images reveal slight dislocation propagation in the microstructures. Thus, the hardness and elastic modulus can be increased slightly after annealing treatment because the existence of comparatively unstable microstructures. It is suggested that cracking phenomena dominate the damage cause of Si/SiGe SLSs.

1. Introduction

Strain-relaxed silicon germanium (SiGe) has become an attractive semiconductor material in recent years because it possesses several attractive properties, including adjustable band gaps, enhanced carrier mobility, and higher dopant solubility than that of pure Si [1–3]. Previous investigations into strained-layer superlattices (SLSs) have led to their use in the development of Si-based micro- and optoelectronic devices [4–8]. Annealing treatment has the potential to reveal reliable quantitative information regarding the behavior of periodic multilayered SiGe structures. There are, however, two key materials aspects limiting the thermal behavior that SiGe can endure during thermal processing: interdiffusion and strain relaxation. These issues also have been observed at previous literatures in term of SiGe interdiffusion [9–14]. Aubertine et al. [15] revealed that three SiGe SLS modes could be prepared using both reduced pressure chemical vapor deposition (RPCVD) and ultrahigh-vacuum chemical vapor deposition (UHVCVD); they suggested that the lattice mismatch of the two semiconductors could be accommodated. The mechanical properties of artificial multilayer films appear to be correlated strongly with their geometrical dimensions [16]. Both misfit dislocations and threading dislocations of crystal defects between the SiGe layer and the Si substrate can induce crystal defects in the microstructure, thereby degrading the quality of the resulting device. SiGe/Si multilayers are useful model systems for investigating film hardness. Indeed, the hardness of such a multilayer film is significantly greater than that of a single monolayer. Indentation techniques can be used to delaminate the films from the substrates and to measure their mechanical properties [e.g., elastic modulus (E) and hardness (H)] [17]. In previous studies [18], it was found that SiGe films exhibit slightly enhanced mechanical properties after thermal annealing, as a result of misfit dislocation propagation. It was also found that high-temperature oxidation treatment leads to strain relaxation in the form of misfit dislocations, which can increase hardness [19]. Meanwhile, we have also been interested in using a commercial nanoindenter to study the mechanical properties of SiGe multilayer films. The hardness of SiGe multilayer films is higher because after annealing treatment misfit dislocations were induced by relaxation effect; they exhibit greater resistance toward plastic deformation relative to corresponding single-layer samples [20]. Such nanomechanical tests have been made possible through the development of instruments that can continuously measure force and displacement [21–27]. Using nanomechanical technology as an analytical

* Corresponding author. Tel.: +886 3 5712121; fax: +886 03 5733409.
E-mail address: a091316104@gmail.com (H.-C. Wen).

0169-4332/$ – see front matter © 2011 Elsevier B.V. All rights reserved.
doi:10.1016/j.apsusc.2011.05.015

tool has several advantages, including free selection of materials, simple design alteration, and convenient initial facilities [28,29]. The values of H and residual stress that are determined this way are significant parameters influencing the applicability of tribological films [30,31].

In this study, a number of growth cycles (nanometer-period) Si/SiGe SLSs layers were prepared and, the effect of annealing on the internal nanomechanical behavior deposited using a UHVCVD was experimentally investigated. A relationship exists between the shear resistance as well as the microstructure can be concluded.

2. Experimental procedure

Multilayer films based on a Si/SiGe superlattice structure were deposited onto a Si substrate using the following procedure: (i) P-type Si(1 0 0) wafers were subjected to a standard Radio Corporation of American (RCA) clean and dipping in a HF:H_2O (1:50) bath for 15 s; they were then introduced into the load-lock chamber of a UHVCVD. (ii) A 10-nm-thick $Si_{0.8}Ge_{0.2}$ layer was deposited at 665 °C for circa 3.6 min from a mixture of pure SiH_4 (85 sccm) and GeH_4 (15 sccm) gases; the deposition rate was 2.8 nm/min under a vacuum of 10^{-7} mbar. (iii) A 6-nm-thick Si buffer layer was immediately deposited on the SiGe layer at 665 °C for 60 min from pure SiH_4 (85 sccm) gas to suppress roughening during annealing; the deposition rate was 0.1 nm/min under a vacuum of 10^{-7} mbar [18–20,32]. (iv) The whole structure was completed by repeating steps (iii) and (iv) 20 times for the preparation of the SLS sample; the total thickness was circa 330 nm. (v) For annealing, the sample was subjected to *ex situ* thermal treatment in a furnace under N_2 gas for 30 min (at 400, 500, or 600 °C). The microstructure of the sample was observed using transmission electron microscopy (TEM, JEOL, JEM-2100F); TEM samples were prepared through mechanical polishing down to 20–30 μm, followed by Ar ion milling to electron transparency; the observations were made at 200 kV.

To investigate the mechanical behavior, nanoindentation measurements were performed using a Nanoindenter MTS NanoXP system (MTS Corporation, Nano Instruments Innovation Center, TN, USA) equipped with a diamond pyramid-shaped Berkovich-type indenter tip (radius of curvature: 50 nm). Stiffness data were recorded along with the load and displacement curve. The values of hardness and Young's modulus of the Si/SiGe superlattice films were calculated from the load–displacement (P–h) data using the analytical method developed by Oliver and Pharr [19]. Each value, reported here together with its standard deviation, resulted from averaging the results of 12 indentations. The thermal drift was maintained below ±0.05 nm/s for all indentations considered herein. A 12 × 1 indentation array was produced with each indentation separated by 50 μm. Using this approach, possible interactions between two consecutive indentation tests were minimized. Each indentation depth was controlled at 100 nm. In each indentation test, the Berkovich diamond indenter was operated with typical-cycle nanoindentation P–h curves; the loading/unloading time was held constantly for 30 s, with the peak load held for 5 s.

To identify the nanotribological properties of the samples, nanoscratch tests were performed using atomic force microscopy (AFM, Digital Instruments Nanoscope III) in conjunction with a nanoindentation measurement system (Hysitron, Inc.). A constant scan speed of 2 μm/s was applied. In order to determine the fracture and abrasion of Si/SiGe SLSs initiated at low-ramped-force modes of sliding cycles, samples with ramped loads of 2000 and 6000 μN were used. With this approach, images corresponding to the surface profiles can be obtained, 10-μm-long scratches were formed in the ramped forces mode. The tip was loaded on the samples ranged from 0 to 2000 μN for both the as-deposited and annealed Si/SiGe SLSs. Surface profiles before and after scratching were obtained by scanning the tip at a normal load of 0.02 mN. After scratching, the wear tracks were imaged through *ex situ* AFM examinations. The coefficient of friction (μ), defined as the ratio of the friction force (F) to the normal force (N) according to Amonton's law [33], is a useful parameter for estimating the nanotribological behavior of coatings and films; plots of μ with respect to the scratch duration were obtained from the AFM analysis.

3. Results and discussion

3.1. Effect of nanoscratch tests of Si/SiGe SLS

The fracture and abrasion of the Si/SiGe SLSs were initiated at low and high ramped forces of the sliding cycles. Fig. 1(a) presents AFM images of Si/SiGe SLSs, grown directly on the Si(0 0 1) substrate without annealing treatment, that had been scratched at two different ramped forces (2000 and 6000 μN); Fig. 1(b)–(d) present images of the corresponding Si/SiGe SLSs after annealing at 400, 500, and 600 °C, respectively. Slight evidence for ramped scratch tracks within the pile up at the end of the scratch functions can be observed. The amount of pile up was influenced by the scratch process and the sliding distance. Fig. 1(c) and (d) reveal marked periodicity (waviness) in the line profiles formed on the annealed samples. In each of the above images, only slight evidence for a scratch track at 2000 μN was observed. In contrast, accumulated small-scale damage was appeared on the Si/SiGe SLSs annealed at 600 °C, resulting from initiation of gross damage to the surface under this ramped force. When the ramped load was set at 6000 μN, increased pile up induced by the higher scratch load was observed upon increasing the sliding distance [34]. This behavior suggests that an observable pure elastic contact occurred at the low ramped force; a slightly machined surface with cracks appeared at the end point, as shown in Fig. 1.

Fig. 2 presents the lateral force plotted with respect to duration of displacement. It can be shown that the applied load increased as the time increased. Fig. 2(a) reveals the normal fluctuations of the lateral force over all of the samples with the distribution in the force value of 2000 μN., However, the samples annealed at 400 and 500 °C exhibited some intermittence of the force value, and the SLS period appears to be reflected by the fluctuation. In Fig. 2(b), unusual lateral force for the sample annealed at 600 °C (force: 6000 μN) was observed. The fluctuation is relative lower than that of the samples annealed at temperatures from 400 to 500 °C. In those cases, the indenter tip jumped forward by an intermission step and then the lateral force was induced gradually while the tip moved backward with the release and build-up of force. Fig. 3(a) and (b) displays typical friction coefficients plotted with respect to the scratch duration for each Si/SiGe SLS under ramped loads of 2000 and 6000 μN. Fig. 3(a) reveals only slightly piled-up scales and fewer sawtooth features in the curve formed for the surface scratched at a ramped load of 2000 μN. This behavior suggests that pure elastic contact dominated at the low ramped force. A slightly machined surface with cracks appeared at the end point. Fig. 3(b) displays typical friction coefficients plotted with respect to the scratch duration (ramped force: 6000 μN) for the samples annealed at the various temperatures. The friction traces were fairly reproducible, but exhibited great variability for each sample. The plots reveal the onset of marked oscillations under the friction force and abrupt oscillations in both the on- and off-load scans. Similar oscillation trends appear for each ramped load. The features in Fig. 3(a) (ramped load was 2000 μN) exhibit more sudden oscillating fluctuations than those in Fig. 3(b) (ramped load was 6000 μN). It is suggested that the lower degrees of adhesion reflect the presence of interlinks and rearrangements that may result in fluctuations of the values of μ (Table 1).

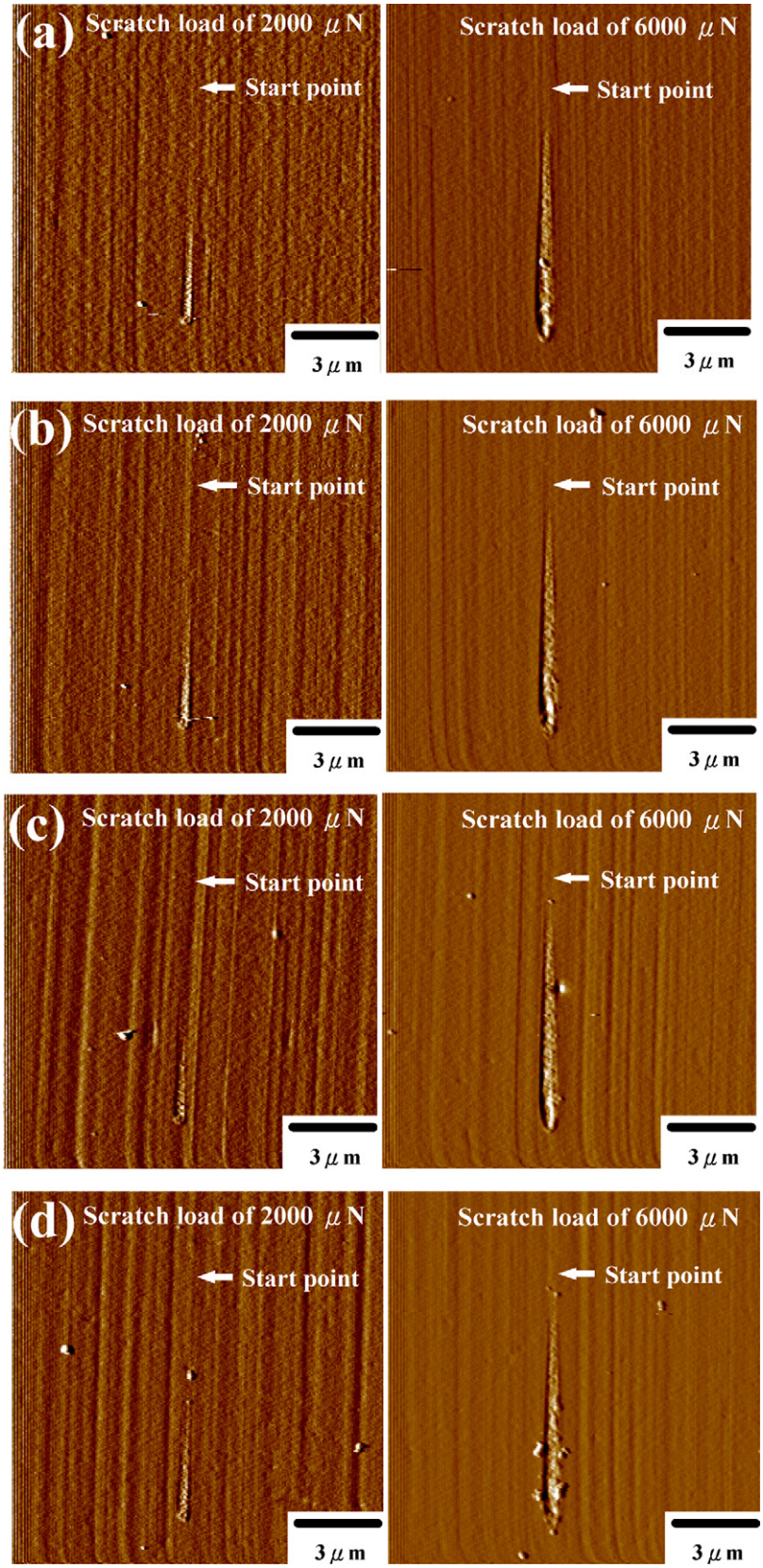

Fig. 1. 3D AFM images of scratch tracks on (a) the as-deposited Si/SiGe SLS and (b–d) Si/SiGe SLSs that had been subjected to thermal treatment at (b) 400, (c) 500, and (d) 600 °C *ex situ* in a furnace under N_2 for 10 min. All samples were scratched under ramped loads of 2000 and 6000 μN.

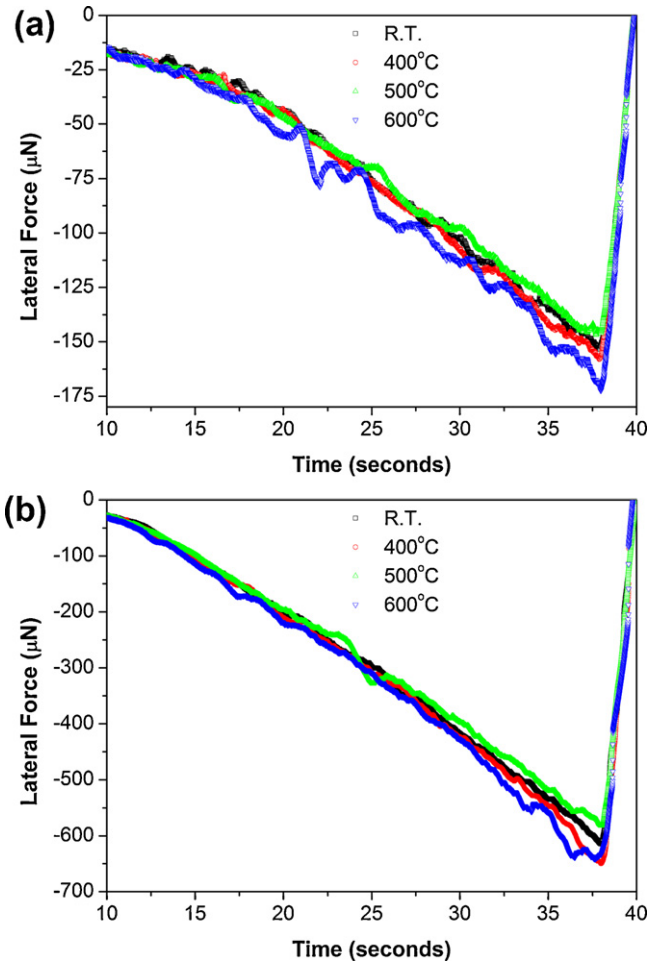

Fig. 2. Typical profiles of the Si/SiGe SLSs, with lateral force plotted with respect to the scratch duration at (a) 2000 and (b) 6000 μN; typical profiles of lateral force [averaged from the measurements in (a) and (b) at scratch durations ranging from 8 to 40 s] plotted with respect to the annealing temperature.

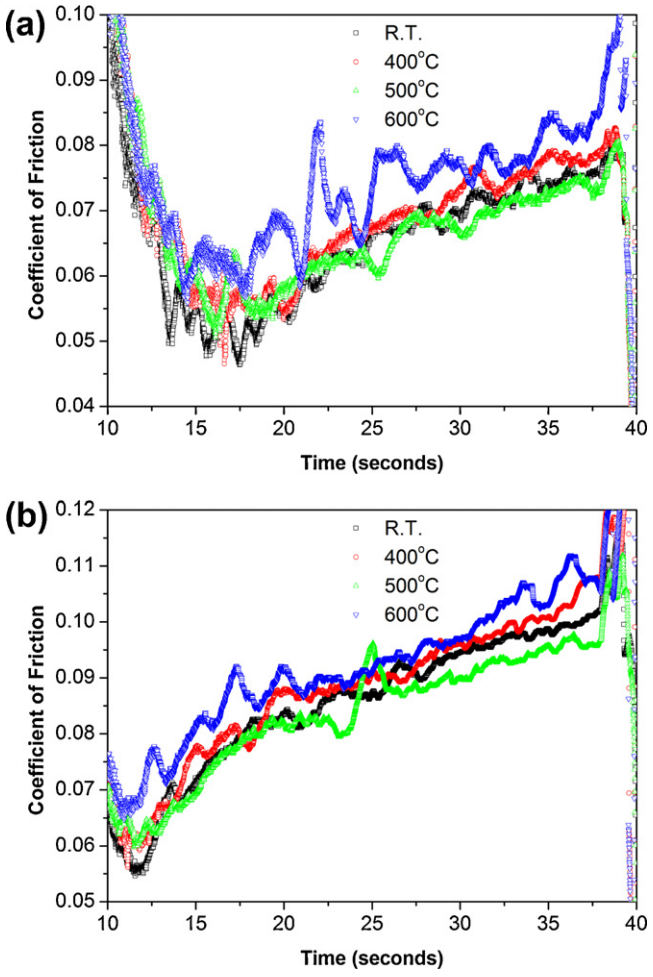

Fig. 3. Typical profiles of the Si/SiGe SLSs, with coefficient of friction (μ) plotted with respect to the scratch duration at (a) 2000 and (b) 6000 μN; typical profiles of μ [averaged from the measurements in (a) and (b) at scratch durations ranging from 8 to 40 s] plotted with respect to the annealing temperature.

3.2. *Effect of nanoindentation tests of Si/SiGe SLS*

The nanoindentation technique is a powerful tool for probing the properties of thin films. The Si/SiGe films were characterized on the nanoscale in terms of their continuous penetration depth by means of continuous stiffness measurement (CSM). Figs. 4 and 5 present the hardness and elastic moduli of the Si/SiGe SLSs, plotted as functions of the indentation depth at 100 nm, following the method proposed by Oliver and Pharr [21]. For indentation depths up to circa 10 nm, the hardness increased as the indentation depth increased. This behavior is usually attributed to the transition between purely elastic to elastoplastic contact, whereby the hardness is the actual contact pressure. The mean contact pressure, when determined under conditions of a fully developed plastic zone, is usually defined as the indentation hardness (Hrt). For indentation depth greater than circa 25 nm, the hardness

Table 1
Loads, coefficients of friction, and lateral forces for the as-deposited Si/SiGe SLS and those subjected to thermal treatment at 400, 500, and 600 °C under typical ramped loads of 2000 and 6000 μN.

Ramp mode	Load (μN)	Coefficient of friction	Lateral force (μ N)
As-deposited	2000	0.075	−69.29
400 °C	2000	0.082	−71.49
500 °C	2000	0.079	−68.50
600 °C	2000	0.086	−76.48
As-deposited	6000	0.088	−273.61
400 °C	6000	0.092	−280.68
500 °C	6000	0.088	−265.83
600 °C	6000	0.096	−290.65

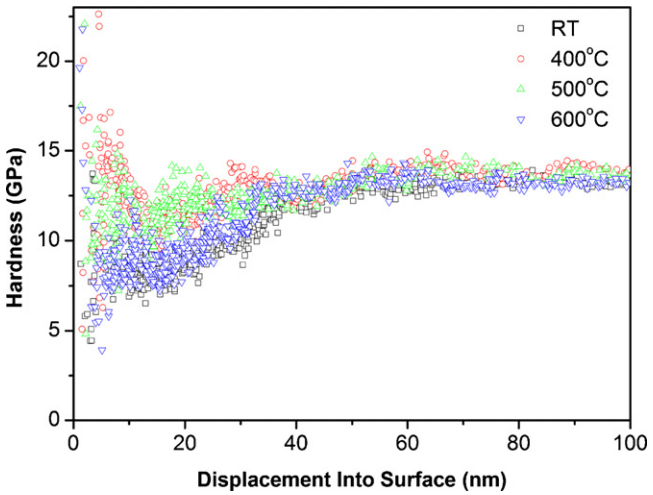

Fig. 4. The values of hardness of the Si/SiGe SLS samples that had been subjected to annealing at (a) RT and at (b) 400, (c) 500, and (d) 600 °C.

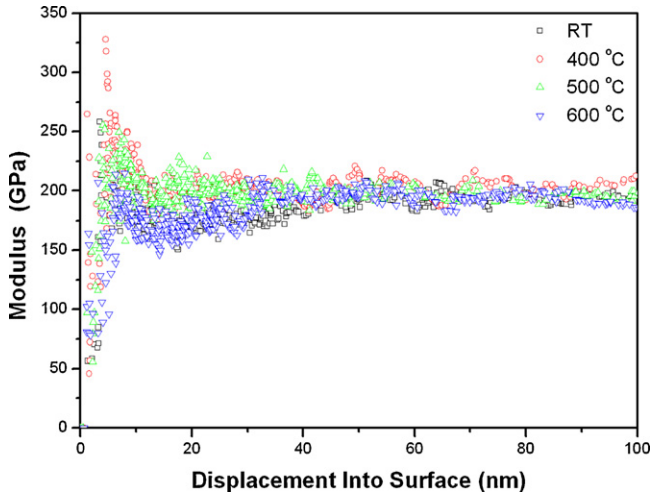

Fig. 5. Elastic moduli of the Si/SiGe SLS samples that had been subjected to annealing at (a) RT and at (b) 400, (c) 500, and (d) 600 °C.

was constant. The plot of the elastic modulus followed a similar trend, except that its magnitude converged at an indentation depth smaller than that for the hardness. The hardness and elastic moduli were evaluated by averaging measurements obtained at indentation depth ranging from 20 to 100 nm – an adequate depth to achieve a fully developed plastic zone without exceeding 45% of the film thickness, to avoid a greater substrate effect [34]. For our Si/SiGe SLSs, the values of hardness were 12.9 ± 0.3, 13.3 ± 0.4, 13.3 ± 0.4, and 13.8 ± 0.5 GPa, respectively, with elastic moduli of 195.2 ± 4.1, 198 ± 4.2, 200 ± 4.2, and 205 ± 5.1 GPa, respectively, at the conditions of as-prepared and annealed at 400, 500, and 600 °C. It is suggested that the slight oscillations and discontinuous phenomena evident in all of the hardness curves might be due to the relaxed Si/SiGe SLS structures. Table 2 compares the relevant mechanical property data (hardness and elastic modulus) from previous reported with those of the three types of SiGe films [18–20]. It is shown that our Si/SiGe SLSs have slightly greater elastic moduli than those of other SiGe films, and typical values of hardness relative to those of SiGe films annealed.

3.3. The microstructure investigation of Si/SiGe SLS

Fig. 6(a) presents the cross-sectional TEM image of the Si/SiGe SLS (20 bilayers, circa 330 nm) that had not been subjected to annealing. A rather thick layer containing structures was formed mainly in the silicon substrate. Fig. 6(b)–(d) display the TEM cross-sectional profiles obtained after annealing. The samples annealed at 400 and 500 °C display smooth interfaces between the Si/SiGe films and the Si substrate, whereas the sample annealed at 600 °C featured significant interdiffusion and misfit dislocations from the bottom of the substrate. These misfit dislocations tend to form serial nucleation seeds and induce high-density dislocation at the interface between the film and the substrate, resulting in the appearance of slip lines. These images allow us to understand why these Si/SiGe SLSs displayed significantly different behavior in the nanoindenter and nanoscratch evaluations.

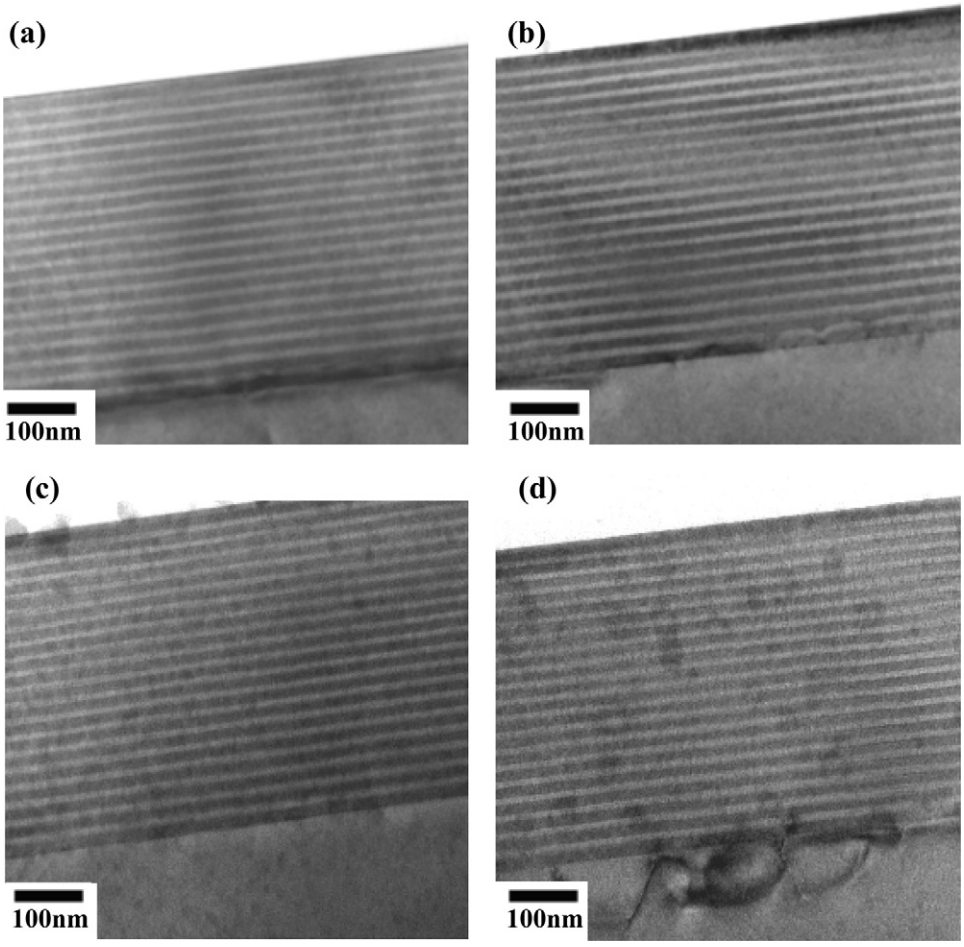

Fig. 6. Cross-sectional TEM images of the Si/SiGe SLS samples that had been subjected to annealing at (a) RT and at (b) 400, (c) 500, and (d) 600 °C.

Table 2
The relevant mechanical property data (hardness and elastic modulus) of previous reported with those of the three types of SiGe films.

	From type	Annealing temperature (°C)	Hardness (GPa)	Young's moduli (GPa)
This study	Si/SiGe Superlattices	RT	12.9 ± 0.3	195.2 ± 4.1
		400	13.3 ± 0.4	198 ± 4.2
		500	13.3 ± 0.4	200 ± 4.2
		600	13.8 ± 0.5	205 ± 5.1
Wen et al. [18]	Single-layer-SiGe	RT	14.5 ± 0.6	–
		800	15.0 ± 0.6	–
		900	16.1 ± 0.4	–
		1000	16.2 ± 0.5	–
Wen et al. [19]	Single-layer-SiGe	RT	12.6 ± 0.4	191.2 ± 6.5
	Multilayer-SiGe	RT	13.7 ± 0.6	194.1 ± 7.9
	Multilayer-SiGe	600	13.9 ± 0.6	184.1 ± 3.2
	Multilayer-SiGe	800	14.2 ± 0.7	189.7 ± 5.3

In the closing, the uncertainty of the initial μ profile, particularly in the low-load region, is associated with the settling down of the indenter head. Hence, scratch deformation on the Si/SiGe films occurring with rather regular oscillations when the ramped load was 6000 μN can be observed. Fig. 3 plots the values of μ of the Si/SiGe SLSs with respect to the annealing temperature. These values were determined by averaging those measured at scratch durations ranging from 12 to 38 s. The as-deposited sample exhibited a relatively low shear resistance to failure at 6000 μN, compared with those of the annealed samples [Fig. 1(a)]. Different critical tracks for the samples annealed at temperatures from 400 to 600 °C can be observed. Under the same conditions, fracture (delamination) events are evident for the annealed samples in Fig. 1(b) and (d). The surface profiles of the regions scanned at 2000 μN confirm that little damage occurred at this low load. The dislocations were formed by corner dislocations, suggesting that SiGe SLSs grown using UHVCVD at low temperature relax through a modified Frank–Reed mechanism [4]. Recent articles [35–37] are suggested that the initial dislocation forms a serial nucleation seed and induces high-density dislocation at the interface of the bulge edge scenarios, thereby creating a serious slip line that can be observed in ours reported. The results in this study are consistent with the nanotribological behavior of Si/SiGe films, in that the as-deposited Si/SiGe SLSs featured more serious component damage (Fig. 1) and oscillation events (Figs. 2 and 3) than did the annealed samples. Therefore, annealing of Si/SiGe SLSs makes them more resistant to plastic deformation, resulting in higher values of μ compared with those of non-annealed samples. During annealing, Si/SiGe SLSs were relaxed to reduce strain energy (Figs. 4 and 5). The restricted dislocation movement, therefore, serves an active role at the interfaces (Fig. 6).

4. Conclusions

A high-quality relaxed Si/SiGe SLSs can be obtained using UHVCVD methods. From AFM, nanoscratch, nanoindenter, and TEM examinations, the following conclusions can be obtained:

i) The deposited Si/SiGe SLS featured marked periodicity (waviness) in their line profiles at 6000 μN, but it was not obvious at 2000 μN.
ii) For all applied loads, the value of μ increased after annealing, presumably because of restricted dislocation movement from the active interfaces after annealing.
iii) The measured values of hardness and elastic moduli of the Si/SiGe films were in the range from 12.9 ± 0.3 to 13.8 ± 0.5 GPa and from 195.2 ± 4.1 to 205 ± 5.1 GPa, respectively. Slight oscillations and discontinuous phenomena in each hardness curve may have been due to the relaxed Si/SiGe structure.
iv) TEM analysis of the SLS structures revealed, from the ramped force of the sliding cycles and the oscillation trends, that the microstructures of the Si/SiGe films/Si were relatively defected after annealing.

Acknowledgments

This study was supported in part by the National Science Council in Taiwan under contract NSC 99-2221-E-009-031-MY2. We thank the National Nano Device Laboratories (contracts NDL99-C03S-042) for technical support. We would like to thank Dr. Ping-Feng Yang and Dr. Yi-Shao Lai (Central Labs, Advanced Semiconductor Engineering) for help with the nanoscratch analysis of SiGe samples and kindly discussion.

References

[1] S.S. Iyer, F.K. LeGoues, J. Appl. Phys. 65 (1989) 4693–4698.
[2] J.M. Baribeau, Appl. Phys. Lett. 57 (1990) 1052–1054.
[3] J.M. Baribeau, J. Appl. Phys. 74 (1993) 3805–3810.
[4] P.M. Mooney, J.L. Jordan-Sweet, K. Ismail, J.O. Chu, R.M. Feenstra, F.K. LeGoues, Appl. Phys. Lett. 67 (1995) 2373–2375.
[5] P.M. Mooney, J.L. Jordan-Sweet, J.O. Chu, F.K. LeGoues, Appl. Phys. Lett. 66 (1995) 3642–3644.
[6] H. Brugger, G. Abstreiter, J. Phys. Colloques. 48 (1987), C5-321-C5-327.
[7] P.M. Mooney, Mater. Sci. Eng. R17 (1996) 105–146.
[8] F. Heinrichsdorff, M.H. Mao, N. Kirstaedter, A. Krost, D. Bimberg, A.O. Kosogov, P. Werne, Appl. Phys. Lett. 71 (1997) 22–24.
[9] S.S. Iyer, F.K. Legoues, J. Appl. Phys. 65 (1989) 4693–4698.
[10] J.M. Baribeau, Appl. Phys. Lett. 57 (1990) 1502–1504.
[11] S. Zheng, M. Kawashima, M. Mori, T. Tambo, C. Tatsuyama, Thin Solid Film 508 (2006) 156–159.
[12] J.M. Baribeau, J. Vac. Sci. Technol. B 16 (1998) 1568–1574.
[13] S.J. Chang, K.L. Wang, Appl. Phys. Lett. 54 (1989) 1253–1255.
[14] S.M. Prokes, O.J. Glembocki, D.J. Godbey, Appl. Phys. Lett. 60 (1992) 1087–1089.
[15] D.B. Aubertine, M.A. Mander, N. Ozguven, A.F. Marshall, P.C. McIntyre, J.O. Chu, P.M. Mooney, J. Appl. Phys. 92 (2002) 5027–5035.
[16] R.C. Cammarata, T.E. Schlesinger, C. Kim, S.B. Qadri, A.S. Edelstein, Appl. Phys. Lett. 56 (1990) 1862–1864.
[17] J. Gong, H. Miao, Z. Peng, Acta Mater. 52 (2004) 785–793.
[18] B.C. He, C.H. Cheng, H.C. Wen, Y.S. Lai, P.F. Yang, M.H. Lin, W.F. Wu, C.P. Chou, Microelectron. Reliab. 50 (2010) 63–69.
[19] B.C. He, H.C. Wen, T.Y. Chiang, Z.C. Chang, D. Lian, W.F. Wu, C.P. Chou, Appl. Surf. Sci. 256 (2010) 3299–3302.
[20] B.C. He, H.C. Wen, M.H. Lin, Y.S. Lai, W.F. Wu, C.P. Chou, Microelectron. Reliab. 50 (2010) 851–856.
[21] J.B. Pethica, R. Hutchings, W.C. Oliver, Philos. Mag. A 48 (1983) 593–606.
[22] W.C. Oliver, G.M. Pharr, J. Mater. Res. 7 (1992) 1564–1583.
[23] M.F. Doerner, W.D. Nix, J. Mater. Res. 1 (4) (1986) 601–609.
[24] J.B. Pethica, in: V. Ashworth, W. Grant, R. Procter (Eds.), Ion Implantation into Metals, Pergamon Press, Oxford, 1982, pp. 147–156.
[25] J.L. Loubet, J.M. Georges, O. Marchesini, G. Meille, J. Tribol. 106 (1984) 43–48.
[26] D. Newey, M.A. Wilkens, H.M. Pollock, J. Phys. E: Sci. Instrum. 15 (1982) 119–122.
[27] D. Stone, W.R. LaFontaine, P. Alexopoulos, T.-W. Wu, C.Y. Li, J. Mater. Res. 3 (1988) 141–147.
[28] L.L. Sohn, R.L. Willet, Appl. Phys. Lett. 67 (1995) 1552–1554.
[29] K. Ashida, N. Morita, Y. Shosida, JSME Int. J. Ser. C 44 (2001) 244–253.

[30] W. Meredith, G. Horsburgh, G.D. Brownlie, K.A. Prior, B.C. Cavenett, W. Rothwell, A.J. Dann, J. Cryst. Growth 159 (1996) 103–107.
[31] C. Jin, B. Zhang, Z. Ling, J. Wang, X. Hou, Y. Segawa, X. Wang, J. Appl. Phys. 81 (1997) 5148–5150.
[32] K. Ismail, F.K. LeGoues, K.L. Saenger, M. Arafa, J.O. Chu, P.M. Mooney, B.S. Meyerson, Phys. Rev. Lett. 73 (1994) 3447–3450.
[33] R.K. Sivamani, J. Goodman, N.V. Gitis, H.I. Maibach, Skin Res. Technol. 9 (2003) 227–234.
[34] V. Jardret, H. Zahousni, J.L. Loubet, T.G. Mathia, Wear 218 (1998) 8–14.
[35] C.Z. Chena, L.H. Liao, C. Li, H.K. Lai, S.Y. Chen, Appl. Surf. Sci. 257 (2011) 2818–2821.
[36] Z.Y. Xuea, X. Wei, B. Zhanga, A. Wu, M. Zhanga, X. Wang, Appl. Surf. Sci. 257 (2011) 5021–5024.
[37] C.Y. Tsao, Z. Liu, X.J. Hao, A. Martin, Green, Appl. Surf. Sci. 257 (2011) 4354–4359.